

November 17, 2021

PERCENTILE-BASED RESIDUALS FOR MODEL ASSESSMENT

Sophie Bérubé¹, Abhirup Datta, Qingfeng Li, Chenguang Wang, Thomas A. Louis

Johns Hopkins Bloomberg School of Public Health, 615 N. Wolfe St.,
Baltimore MD 21205

Abstract

Residuals are a key component of diagnosing model fit. The usual practice is to compute standardized residuals using expected values and standard deviations of the observed data, then use these values to detect outliers and assess model fit. Approximate normality of these residuals is key for this process to have good properties, but in many modeling contexts, especially for complex, multi-level models, normality may not hold. In these cases outlier detection and model diagnostics aren't properly calibrated.

Alternatively, as we demonstrate, residuals computed from the percentile location of a datum's value in its full predictive distribution lead to well calibrated evaluations of model fit. We generalize an approach described by Dunn and Smyth (1996) and evaluate properties mathematically, via case-studies and by simulation. In addition, we show that the standard residuals can be calibrated to mimic the percentile approach, but that this extra step is avoided by directly using percentile-based residuals. For both the percentile-based residuals and the calibrated standard residuals, the use of full predictive distributions with the appropriate location, spread and shape is necessary for valid assessments.

KEYWORDS

Percentile-based residuals, Model assessment, Outlier detection, non-Gaussian predictions, Well-calibrated diagnostics.

1 Introduction

Residuals are a key component of diagnosing model fit. They are used to identify outlying data points, and plotted against predicted values they can reveal model lack of fit. The commonly used standard residuals are computed as, $\text{Residual} = (\text{Observed} - \text{Expected})/\text{SD}$, where the

¹Contact author: sberube3@jhmi.edu

‘Expected’ and ‘SD’(standard deviation) come from a data point-specific predictive distribution. Irrespective of model form, if the predictive distributions are well estimated, these residuals have mean 0 and variance 1, however there is no guarantee that they will have a $N(0, 1)$ distribution. If they aren’t $N(0, 1)$, outlier detection and global model assessments can perform poorly, with poorly calibrated Type I error for outlier detection, potentially low power, and misleading residual plots. Therefore, a residual that is well-calibrated for any predictive distribution has the potential to improve performance, and a percentile-based approach achieves this goal. Herein, we develop and evaluate a generalization of Dunn and Smyth (1996). Expanding on their randomized percentile-based residual, we consider an approach that goes beyond the first two moments of the full predictive distribution and uses all data points to derive the full predictive distribution, which is then used in its entirety to compute the percentile-based residuals. We further derive mathematical properties of these percentile-based residuals including their power.

Percentile-based residuals are computed by finding the percentile location of an observation in its full predictive distribution, then computing the corresponding Gaussian quantile to produce the residual. For continuous distributions, when the full predictive distribution matches the underlying truth, these residuals are distributed $N(0, 1)$. The definition is general in that the full predictive distribution can be from a Bayesian analysis (including using the MCMC draws as the distribution), from frequentist modeling, from machine learning (e.g. classification and regression trees (CART), support vector machines, etc.) or from any other modeling approach. More recent work on this topic includes Cook et al. (2006) describing the ‘percentile, and Gaussian quantile’ approach to evaluating computer software and Efron (2008) who presents an example of transforming to z-values. The use of inverse Gaussian transformations was introduced much earlier than 2006 though, with Efron (1987) showing an example of the ability of normalizing inverse transformations to automatically improve performance of the bootstrap confidence intervals without the user having to re-calibrate the process for each new

application.

With ‘SD’, the standard deviation of the predictive distribution, if the working predictive distribution is Gaussian, the standard (Observed - Expected)/SD residuals are identical to the percentile-based residuals. However, the Gaussian assumption is commonly inappropriate. For instance, Dunn and Smyth (1996) consider a log-linear model in the context of survival data as well as a logistic regression in the context of binomial data. Rather than these examples, we consider models for which the full predictive distribution may incorporate parameter uncertainty, and hierarchical models with distributions that aren’t Gaussian. We show that in such cases, assuming normality, and using the standard residuals can lead to poorly calibrated model diagnostics and outlier detection; in the context of formal hypothesis testing, conservative or inflated Type I errors and similar influences on the power of the test. Against this background, we show that replacing the standard residuals by the percentile-based properly calibrates model assessment and testing. Similar advantages are associated with using percentile-based residuals in diagnostic plots. Finally we show that the usual residuals can be calibrated to mimic the percentile-based approach, but this step is avoided by direct use of percentiles.

2 Notation and Methods

Let (Y_k, \mathbf{X}_k) represent all data (dependent variable, covariates) for the k^{th} ($k = 1, \dots, K$) sampling unit, and let (\mathbf{Y}, \mathbf{X}) represent all data. We focus on a scalar Y_k , which can be a unit-specific summary statistic. The analyst produces a working model, $[Y_k | \mathbf{X}_k, \boldsymbol{\psi}]_{\text{wkng}}$ with covariates \mathbf{X}_k and parameters $\boldsymbol{\psi}$ (all parameters; slopes, variances, variance components, etc.). Embedded in the working model are all modeling assumptions and data analytic choices. Examples include linear and logistic regression, CART, random forests and other machine learning approaches (for these $\boldsymbol{\psi}$ represents the underlying algorithm’s end result). Data analysis produces

the working predictive cumulative distribution function for unit k ,

$$D_k(Y_k) = D_k(Y_k | \mathbf{X}_k, \text{Analysis}), \quad (1)$$

but the true predictive cumulative distribution function for the k^{th} unit is,

$$F_k(Y_k) = F(Y_k | \mathbf{X}_k). \quad (2)$$

D_k is determined by the the modeling approach, and producing it is quite general. The full posterior distribution of $\boldsymbol{\psi}$ can be used to generate an in or out of sample predictive distribution for Y_k (e.g., the collection of MCMC samples), a plug-in approach substituting $\hat{\boldsymbol{\psi}}$ for $\boldsymbol{\psi}$ with no attention to uncertainty in the estimate, or the end-result of a machine-learning algorithm, with or without infusion of uncertainty.

2.1 The (O - E)/SD, or standard residuals

With $Y_k = y_k$, the standard (Observed - Expected)/SD residuals are,

$$\begin{aligned} R_k^* &= \frac{y_k - \mu_k}{\sigma_k} \\ \mu_k &= E_{D_k}(Y_k | \mathbf{X}_k) \\ \sigma_k^2 &= V_{D_k}(Y_k | \mathbf{X}_k) \end{aligned} \quad (3)$$

An example of the above residual is linear regression, where $R_k^* = \frac{y_k - \hat{y}_k}{\sqrt{\text{MSE}}}$. In order to perform model diagnostics like outlier identification and goodness of fit, the empirical distribution of the R_k^* is evaluated relative to the $N(0, 1)$ distribution; plotting R_k^* versus μ_k can identify the need for model enhancement. If (μ_k, σ_k) are the true mean and standard deviation under F_k , then the R_k^* have mean 0 and variance 1, but the full distribution can be far from Gaussian unless the Y s are Gaussian or approximately Gaussian due to the Central Limit Theorem (CLT).

2.2 Percentile-based residuals

The standard residuals can be represented as,

$$R_k^* = \Phi^{-1} \{ \Phi_{\mu_k, \sigma_k}(y_k) \}, \quad (4)$$

where $\Phi_{\mu,\sigma}$ denotes the CDF, or cumulative density function, of a $N(\mu, \sigma^2)$ distribution and $\Phi = \Phi_{0,1}$. This framework supports generalizing the definition of a residual by using the full predictive distribution of Y_k . To relax dependence on the CLT, we find the percentile location of $Y_k = y_k$ in the working predictive distribution D_k and map it to the associated quantile of a $N(0, 1)$ distribution. Specifically, we define

$$\begin{aligned} R_k^\ddagger &= \Phi^{-1} \{D_k(y_k)\} \quad (\text{for continuous } D_k), \\ &= \Phi^{-1} \{D_k(y_k) - 0.5\text{pr}_{D_k}(Y_k = y_k)\} \quad (\text{for discrete } D_k). \end{aligned} \tag{5}$$

The ‘one-half correction’ is needed to balance the computation for a discrete distribution. For example, if D_k puts all mass at a single point and y_k is that point, the uncorrected $R_k^\ddagger = \infty$; the corrected (and correct) $R_k^\ddagger = 0$. If the direct estimate, y_k , is equal to the largest value of the predictive distribution, the correction brings R_k^\ddagger from infinity to a finite value. Even for a continuous D_k , either R_k^* or R_k^\ddagger can be $\pm\infty$, for example if the observed value is beyond the support of the predictive distribution. In these cases, truncating the residual, for example at ± 5.0 , is often appropriate.

Equation 5 is equivalent to replacing Φ_{μ_k, σ_k} in equation 4 with the predictive distribution D_k . It is also evident that when D_k is Gaussian, the standard residuals are identical to the percentile-based. Importantly, this approach allows the user to estimate the working predictive distribution, and thus the residuals, using all data points.

3 Properties

The data analyst generates the working predictive distribution D_k using data from K units with n_k observations in unit k . The n_k can be small and so the unit-specific, direct estimates, y_k may be far from Gaussian. Thus, assuming that the R_k^* are $N(0, 1)$ may induce false positive and false negative rates far from the nominal values in assessing the relation between the observed and expected values. More generally, when each

$D_k = F_k$, the empirical distribution of (R_1^*, \dots, R_K^*) can deviate substantially from $N(0, 1)$.

Dropping the subscript k with the understanding that the distributions are k -specific, we evaluate properties under $H_0 : F = D$ and under $H_1 : F \neq D$. A discrepancy between F and D detected under H_0 is a Type I error (a false positive) and failing to detect a discrepancy between F and D under H_1 is a Type II error (a false negative). Discrepancies between F and D can be induced by various conditions including the use of incorrect parametric families, an incorrect mean model, the lack of uncertainty infusion or some combination of these. In analyzing residuals, the goal is to detect discrepancies between F and D while controlling Type I error, optimizing power and producing valid and informative residual plots. We show herein that depending on the choice of D the use of standard residuals (R^*) can cause Type I error rate to be inflated or conservative and the shape of the true predictive distribution, F , can be mis-represented.

3.1 Properties of R^*

Let μ_0 and σ_0 denote the mean and variance of D . We first show that the Type I error for the standard residuals is not well calibrated.

Theorem 1. *[Type I error] The Type I error at level α for standard residuals, R^* is given by:*

$$\alpha^*(\alpha) = \begin{cases} 1 - \Phi_{\mu_0, \sigma_0}\{D^{-1}(1 - \alpha)\} & \text{for right sided test} \\ \Phi_{\mu_0, \sigma_0}\{D^{-1}(\alpha)\} & \text{for left sided test} \\ \text{unique root of: } 1 - D(\Phi_{\mu_0, \sigma_0}^{-1}(1 - x/2)) + D(\Phi_{\mu_0, \sigma_0}^{-1}(x/2)) - \alpha = 0 & \text{for two sided test} \end{cases} \quad (6)$$

Proof: We give the proof for the right sided test. Let $U^* = \Phi\left(\frac{Y - \mu_0}{\sigma_0}\right)$, then

$$\begin{aligned}
\text{pr}(U^* \geq 1 - t) &= 1 - \text{pr} \left\{ \Phi \left(\frac{Y - \mu_0}{\sigma_0} \right) \leq 1 - t \right\} \\
&= 1 - \text{pr} \{ Y \leq \Phi_{\mu_0, \sigma_0}^{-1}(1 - t) \} \\
&= 1 - D \{ \Phi_{\mu_0, \sigma_0}^{-1}(1 - t) \}.
\end{aligned}$$

So, the effective Type I error for the standard residuals is

$$\alpha^*(\alpha) = 1 - D \{ \Phi_{\mu_0, \sigma_0}^{-1}(1 - \alpha) \}. \quad \square$$

The proof for the left-sided test is essentially the same as for the right-sided; the proof for the two-sided test combines the right and left tail probabilities.

From Theorem 1, it follows that the Type I error for a right-sided test using R^* induces the following relationships to the nominal level, α :

$$\begin{aligned}
\text{Inflated} &\iff D\{\mu_0 + \sigma_0\Phi^{-1}(1 - \alpha)\} < (1 - \alpha) \text{ or } \Phi_{\mu_0, \sigma_0}^{-1}(1 - \alpha) < D^{-1}(1 - \alpha) \\
\text{Exact} &\iff D\{\mu_0 + \sigma_0\Phi^{-1}(1 - \alpha)\} = (1 - \alpha) \text{ or } \Phi_{\mu_0, \sigma_0}^{-1}(1 - \alpha) = D^{-1}(1 - \alpha) \\
\text{Conservative} &\iff D\{\mu_0 + \sigma_0\Phi^{-1}(1 - \alpha)\} > (1 - \alpha) \text{ or } \Phi_{\mu_0, \sigma_0}^{-1}(1 - \alpha) > D^{-1}(1 - \alpha)
\end{aligned} \tag{7}$$

It is now easy to identify the conditions that lead to inflated or conservative Type I error. If D places more probability mass on the right-tail than the Gaussian distribution, the standard residuals will produce inflated Type I error. Conversely, if D places less probability mass on the right-tail than the Gaussian distribution, then the standard residuals will produce conservative Type I error. Similar conditions can be derived for left- and two-sided tests.

The proof of Theorem 1 immediately identifies the raw power of R^* under H_1 , where ‘raw’ indicates that the power is not adjusted for the poorly calibrated Type 1 error.

Theorem 2 (Power for R^*). *R^* has power for rejection to the right with nominal right-sided Type I error α ,*

$$POW_F^*(\alpha) = 1 - F\{\mu_0 + \sigma_0\Phi^{-1}(1 - \alpha)\} = 1 - F(\Phi_{\mu_0, \sigma_0}^{-1}(1 - \alpha)) \tag{8}$$

3.2 Properties of R^\ddagger

For continuous F and D ,

$$\begin{aligned} \text{pr}_F(D(Y) \leq u) &= \text{pr}\{Y \leq D^{-1}(u)\} = F\{D^{-1}(u)\} \\ &= u, \text{ if } D = F. \end{aligned} \quad (9)$$

Consequently, under H_0 when $D = F$, $R^\ddagger \sim N(0, 1)$, and Type I error using the right-sided rejection region $(\Phi^{-1}(1 - \alpha), \infty)$ is perfectly calibrated.

Theorem 3 gives the full distribution of R^\ddagger for the continuous case.

Theorem 3. [Distribution of R^\ddagger] For continuous F and D with densities f and d , let G_F^\ddagger be the distribution of R^\ddagger with density g_F^\ddagger computed under F . Then, if F is absolutely continuous wrt D ,

$$\begin{aligned} G_F^\ddagger(r) &= F[D^{-1}\{\Phi(r)\}] \\ g_F^\ddagger(r) &= \phi(r) \frac{f[D^{-1}\{\Phi(r)\}]}{d[D^{-1}\{\Phi(r)\}]}. \end{aligned} \quad (10)$$

Consequently, if $D = F$, $g_F^\ddagger(r) = \phi(r)$.

Proof.

$$R^\ddagger = \Phi^{-1}\{D(Y)\}$$

so,

$$\begin{aligned} G_F^\ddagger(r) &= \text{pr}(R^\ddagger \leq r) = \text{pr}\{\Phi^{-1}(D(Y)) \leq r\} = \text{pr}\{D(Y) \leq \Phi(r)\} \\ &= \text{pr}[Y \leq D^{-1}\{\Phi(r)\}] = F[D^{-1}\{\Phi(r)\}] \end{aligned}$$

Taking the derivative wrt r gives the density in equation (10). \square

From equation (10), for g_F^\ddagger to be a Gaussian density, the ratio must be 1.0 (as it is under H_0). More generally, $g_F^\ddagger(r)$ contains $\phi(r)$ as a multiplicative factor which can produce a Gaussian-like shape.

3.3 Power comparisons

We begin by deriving power (e.g., probability of detecting an outlier) for the right-sided test at level α .

Theorem 4 (Power for R^\ddagger). *The right-side rejection power of R^\ddagger for a one-sided test of nominal (and actual) size α is,*

$$POW_F^\ddagger(\alpha) = 1 - F\{D^{-1}(1 - \alpha)\} \quad (11)$$

Proof. Substitute $r = \Phi^{-1}(1 - \alpha)$ in equation 10. □

Using equations 8 and 11 various comparisons can be made between the standard residuals (R^*) and the percentile-based residuals (R^\ddagger). For a right-sided test, since F is monotonically increasing, R^* will have higher, equal or less power than R^\ddagger depending on whether $\Phi_{\mu_0, \sigma_0}^{-1}(1 - \alpha)$ is less than, equal to, or greater than $D^{-1}(1 - \alpha)$. Combining the power comparisons with the results for the Type I error of R^* in (1) we have the following result:

Theorem 5. *For a right-sided test, the standard residuals have inflated, correct, or conservative Type I error, and higher, equal, or lesser power than R^\ddagger depending on whether $\Phi_{\mu_0, \sigma_0}^{-1}(1 - \alpha)$ is less than, equal to, or greater than $D^{-1}(1 - \alpha)$.*

The result shows why it is inappropriate to use the standard residuals. When $\Phi_{\mu_0, \sigma_0}^{-1}(1 - \alpha) < D^{-1}(1 - \alpha)$, R^* may have higher power than R^\ddagger , but that apparent win is induced at least in part by inflated Type I error. On the other hand, when $\Phi_{\mu_0, \sigma_0}^{-1}(1 - \alpha) > D^{-1}(1 - \alpha)$, R^* will have conservative Type I error and lower power than R^\ddagger . By contrast, the R^\ddagger have properly calibrated Type I error and valid power. Importantly, even with well calibrated percentile-based residuals, multiple testing corrections should be performed when appropriate.

3.3.1 Calibrating R^*

The R^* can be adjusted to have properly calibrated Type I error and thus valid power. From Theorem 1, using a right-sided rejection region of the form $(\Phi^{-1}(1 - \alpha^*), \infty)$, R^* gives a Type I error of $1 - D\{\Phi_{\mu_0, \sigma_0}^{-1}(1 - \alpha^*)\}$. Equating this to the nominal level α we have:

$$\alpha^* = 1 - \Phi_{\mu_0, \sigma_0}\{D^{-1}(1 - \alpha)\}. \quad (12)$$

Constructing the right-sided rejection region based on the the $(1 - \alpha^*)^{th}$ quantile now gives a test based on usual residuals with calibrated Type I. As Theorem 6 shows, the power for the calibrated R^* equals the power for the percentile-based residuals.

Theorem 6. *For the right-sided test, the power of the calibrated R^* equals that of R^\ddagger .*

Proof. From equation 8, the power for the right-sided test based on R^* using calibrated rejection region is given by $1 - F\{\Phi_{\mu_0, \sigma_0}^{-1}(1 - \alpha^*)\}$. Using the definition of α^* from equation 12, this gives $1 - F\{D^{-1}(1 - \alpha)\}$, which is the power for the percentile-based residuals from equation 11. \square

This power equivalence also holds for a left-sided test, but does not hold exactly for a two-sided.

Theorems 5 and 6 illustrate the pitfalls of using the standard residuals and highlight the importance of using the full, predictive distribution for model assessment, via either R^\ddagger or the calibrated R^* .

4 Simulation study

We conducted a simulation study to evaluate and compare properties of R^* (both uncalibrated and calibrated) and R^\ddagger .

4.1 Data generation

For $Y_k \sim \text{Beta}(a_k, b)$, $b \equiv 3$, $\log(a_k) = \beta_0 + \beta_1 X_{k,1} + \beta_2 X_{k,2}$, $X_{k,1} \sim N(0, 1)$ and $X_{k,2} \sim \text{Bernoulli}(0.5)$, we consider two *true* models, $F_k^{(0)}$ and $F_k^{(1)}$. For each model, $\beta_0 = 0, \beta_1 = 1$. For $F_k^{(0)}$, $\beta_2 = 0$; for $F_k^{(1)}$, $\beta_2 = -5$. $F_k^{(0)}$ and $F_k^{(1)}$ can be interpreted as the cumulative distribution under the null and alternative hypotheses, respectively.

In the working model (D_k) , (b, β_0, β_1) are unknown, and $\log(a_k) = \beta_0 + \beta_1 X_{k,1}$. Bayesian analysis produces the working predictive distribution $D_k(Y_k)$ based on the collection of the MCMC samples of Y_k . Specifically, $(\beta_0, \beta_1) \text{ ind } N(0, 100)$ and $b \sim \text{Uniform}(0, 5)$. A total of 2000

iterations were obtained with 1000 burn-in. The convergence was checked visually by the trace plot as well as the Gelman-Rubin convergence statistic (Gelman et al., 1992).

4.2 Results

Based on a single replication of $K = 1,000$ sampling units, Figure 1 compares R^* and R^\ddagger from the working model D under the true models $F^{(0)}$ (the null hypothesis) and $F^{(1)}$ (the alternative hypothesis). Note that under the null (the left column), the distribution of R^\ddagger is very close to the $N(0, 1)$ reference, which is not the case for R^* , indicating that R^* is poorly calibrated. Also, under the alternative (right column) R^\ddagger is more likely to detect a model discrepancy than is R^* .

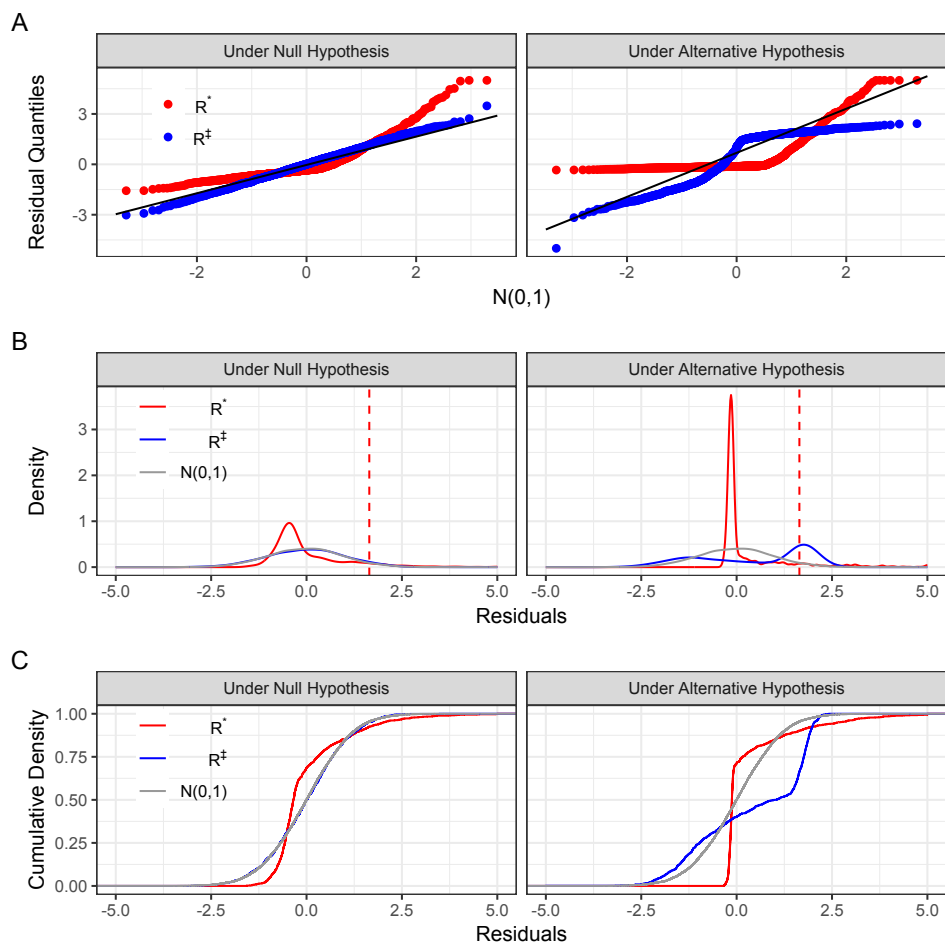


Figure 1: R^\dagger and R^* based on a single replication of 1,000 sampling units. Panel A, Q-Q plots; panel B, smoothed densities; Panel C, empirical CDFs. Panel A includes the reference $y = x$ line (black). Panels B and C include the reference $N(0, 1)$ density and distribution. The vertical dashed line in Panel B corresponds to the right-sided rejection region for $\alpha = 0.05$. The reference $N(0, 1)$ line overlaps with R^\dagger in the left column (null hypothesis) in Panels B and C.

Table 1 reports the estimated rejection rate based on 1,000 replications of the null hypothesis where the *true* residual of a sampling unit is 0, with nominal, right-sided $\alpha = .05$ for R^\ddagger , R^* , and calibrated R^* with α^* from equation 12. Type I error is inflated for R^* , but neither for R^\ddagger nor for calibrated R^* . All simulations produce similar comparisons.

True Model	Hypothesis	N	Rejection Rate			Calibrated $\alpha^*(0.05)$
			R^*	R^* (calibrated)	R^\ddagger	
$F^{(0)}$	Null	150	0.074	0.050	0.049	0.026
		175	0.074	0.050	0.050	0.026
		200	0.074	0.050	0.050	0.026
		225	0.074	0.050	0.050	0.026
		250	0.073	0.050	0.049	0.026
$F^{(1)}$	Alternative	150	0.103	0.324	0.321	0.428
		175	0.103	0.326	0.323	0.429
		200	0.102	0.326	0.324	0.430
		225	0.102	0.319	0.316	0.424
		250	0.102	0.323	0.320	0.426

Table 1: Estimated rejection rate based on 1,000 replications with right-sided $\alpha = 0.05$ for R^\ddagger , R^* , and calibrated R^* using α^* from equation 12.

5 Application to Protein Microarrays

When a protein microarray is assembled, probes or specific proteins are arranged in rows and columns on a glass slide. After the sample of interest has been loaded onto the slide, the array is scanned and light of different wavelengths produces a signal at each probe the intensity of which depends on the presence and quantity of a particular target protein in the sample. The scanning apparatus for protein microarrays produces two measurements at each probe: an observed foreground, signal Y_{fg} and an observed background signal, Y_{bg} . We present simulated arrays composed of 10,000 individual foreground and background signals generated under three conditions. Generally, the goal of this simulation is to compare a case where the analysis model incorporates more variability than is in the data

generating model and a case where the analysis model and the data generating model match exactly. In this sense, we aim to show how percentile-based residuals can effectively assess general model fit.

5.1 Model and estimation

In this simulation, we posit that that a true underlying foreground signal, S , and a true underlying background signal, B , multiply to produce a true, underlying quantity, $S \times B$. In the protein array, B and $S \times B$ are measured with multiplicative errors e_{bg} and e_{fg} to produce Y_{bg} and Y_{fg} . Measurement errors e_{fg} and e_{bg} are independent, log-normal with $\sigma_{bg}^2, \sigma_{fg}^2$ the respective variances of the underlying normal distributions.

These assumptions are encoded in the Bayesian hierarchical model (the analysis model, D),

$$\begin{aligned}
 Y_{bg}|B &\sim \text{log-normal} \left\{ \log(B) - \frac{\sigma_{bg}^2}{2}, \sigma_{bg}^2 \right\} \\
 Y_{fg}|S, B &\sim \text{log-normal} \left\{ \log(B \times S) - \frac{\sigma_{fg}^2}{2}, \sigma_{fg}^2 \right\} \\
 S &\sim \text{gamma}(\alpha_s, \beta_s), \alpha_s = \frac{\mu_s^2}{\sigma_s^2}, \beta_s = \frac{\mu_s}{\sigma_s^2} \\
 B &\sim \text{gamma}(\alpha_b, \beta_b), \alpha_b = \frac{\mu_b^2}{\sigma_b^2}, \beta_b = \frac{\mu_b}{\sigma_b^2} \\
 \mu_s, \mu_b &\sim \text{uniform}(0, 10^6) \\
 \sigma_s^2, \sigma_b^2 &\sim \text{uniform}(0, 10^8)
 \end{aligned} \tag{13}$$

We performed simulations by generating 10,000, or an array's worth of foreground and background signals on a three-tiered basis for the true distribution (F). Tier 1 involves fixing a single $S = 6,000$ and $B = 60$, Tier 2 involves fixing $\alpha_s = \alpha_b = \beta_s = \beta_b = 1$ (not shown below), and Tier 3 involves randomly generating $\alpha_s, \alpha_b, \beta_s, \beta_b$. The analysis model (D , equation 13) matches Tier 3. In all tiers, $\sigma_{bg}^2 = \sigma_{fg}^2 = 0.1$.

We report results for Tier 1 and Tier 3 (results for Tier 2 are very similar to those for Tier 1). The analysis model is used to generate MCMC draws

from relevant posterior distributions. For each MCMC, three chains were run with randomly selected initial values for all parameters with a burn-in of 2,000 and a subsequent 10,000 iterations with a thinning interval of length 10, resulting in a sample size of 1,000 for each of the 10,000 simulated probes on an array. The convergence was checked visually by the trace plot as well as the Gelman-Rubin convergence statistic (Gelman et al., 1992).

5.2 Analysis of residuals

We define the standard residual and the percentile-based residual in this context as follows:

$$\begin{aligned} R_i^* &= \frac{Y_{fg,i} - E[Y_{fg,i}|\text{model}(D)]}{\sqrt{\text{Var}[Y_{fg,i}|\text{model}(D)]}} \\ R_i^\ddagger &= \Phi_{0,1}^{-1}[\text{percentile location of } Y_{fg,i} \text{ in } \text{Pred}_i\{\text{model}(D)\}] \end{aligned} \tag{14}$$

In this case, ‘ D ’ is all generated data points, $\text{model}(D)$ is the model described in 13 estimated using D , and $\text{Pred}_i\{\text{model}(D)\}$ is the full predictive distribution of $[Y_{fg,i}|\text{model}(D)]$. Note that best practice would be to set aside the i th observation, fit the model and use it to predict the i th data value using $\text{model}(D_{-i})$. However, with the large sample size in our example, the difference is negligible.

While in Tier 3, the analytic and data-generating models match, in Tier 1, the analytic model brings in more stochastic elements than are present in the data. This discrepancy is clearly displayed in panel B of Figure 2. The percentile-based residuals of the true Y_{fg} values in the posterior predictive distribution $Y_{fg,i}|\text{model}(D)$ have a standard normal distribution in Tier 3, whereas the percentile-based residuals in Tier 1 have a much narrower spread and are centered slightly to the left of zero.

Importantly, in Tier 3, where the data analysis model and the data generation model match exactly, the standard residuals, R^* depart from the standard normal distribution. As evidenced clearly in Panel A of

figure 2 the quantiles of the standard residuals as compared to the $N(0, 1)$ quantiles would lead to an inflated Type I error rate, that is a higher probability of erroneously detecting a discrepancy between the true predictive distribution and the working predictive distribution.

6 Sub-national estimates of contraceptive use

Access to family planning provides multi-faceted benefits to women and their families. It has been shown to reduce maternal and child mortality, empower women and girls, and enhance environmental sustainability. Remarkable progress has been made in the past several decades in measuring family planning use rates around the world, and in low-income countries in particular. However, the national focus of those surveys (e.g., Demographic and Health Surveys) makes the result impractical for monitoring and evaluation at sub-national levels. Given the fact that many policies are made and implemented at subnational levels, there is an urgent need to reach out to policy makers at local levels and empower them with relevant estimates.

6.1 The Performance Monitoring and Evaluation 2020 Survey

The data analyzed here are drawn from Performance Monitoring and Evaluation 2020 (PMA2020) survey conducted in Kenya during May-July of 2014. The survey interviewed 3479 women in 111 enumeration areas (EAs) in Kenya. Funded by the Bill and Melinda Gates Foundation, PMA2020 was originally designed to facilitate annual progress reporting in support of the goals and principles of Family Planning 2020 (FP2020) initiative across priority countries in Africa and Asia (Zimmerman et al., 2017). The survey uses mobile devices (smartphones) to routinely gather nationally representative data on key family planning indicators. Data are collected at the woman, household, and facility levels by a network of resident enumerators stationed throughout the country.

Given its original goal of providing national estimates, PMA2020 surveys are adequately powered to provide reliable estimates for the whole nation, and in some cases for urban and rural regions separately. While national estimates become more available, regional, county and district officials expressed interests in estimates of indicators to monitor and evaluate progress at their level of operation and responsibilities. To meet this need, a Bayesian hierarchical model was developed for several African countries with multiple rounds of PMA surveys (Li et al., 2019). Described below is a model for a single cross-section of the repeated cross-sectional data collected in that study. The sufficiently large number of women per EA (about 30) makes the standard and percentile-based residuals nearly identical, and to illustrate the difference between the two, we present results based on a 30%, unstratified random sample of the original PMA dataset.

6.2 Bayesian Modeling

$Y_{ik} = 0/1$ is the indicator of woman i in EA k ($i = 1, \dots, n_k; k = 1, \dots, K$) not using (0) or using (1) contraceptive methods. X_{ik} is the woman-specific vector of covariates (e.g., age, education, parity), and $U_k \sim N(0, \tau^2)$ is an EA-specific random effect. The working model is,

$$\begin{aligned} P_{ik} &= \text{pr}(Y_{ik} = 1 \mid X_{ik}, \beta, U_k = u_k) \\ \text{logit}(P_{ik}) &= X_{ik}\beta + u_k. \end{aligned}$$

The P_{ik} are ‘rolled up’ to the EA level (producing P_{+k}), and these are the model-based, EA-specific rates.

As described in Li et al. (2019), we used Markov chain Monte Carlo implemented using JAGS (version 4.3.0) and conducted in R, to generate draws from the joint posterior distribution of $(\beta, \tau^2; U_1, \dots, U_K)$, and consequently for P_{ik} and P_{+k} , the latter being ‘Small Area Estimates.’ The quantity ‘Avelogistic’ is produced by mixing the P_{ik} over the posterior for (β, τ^2) , but over the mixture of $N(0, \tau^2)$ priors for U_k . This approach

produces residuals relative to a population model rather than those relative to a model tuned to the EA, and so evaluates model adequacy.

6.3 Data Analysis

Figure 3 shows the percentile-based and standardized residuals for the 111 EAs. The variation in percentile-based residuals is smaller than in standard residuals (Panel A). Panel B suggests that both R^* and R^\ddagger are close to normally distributed, that each set has a variance greater than 1.0, with the percentile-based having a smaller spread. Panel C reveals additional detail, showing that the R^* are close to Gaussian (albeit with a large spread), but the R^\ddagger are bimodal, possibly indicating that a binary covariate is missing from the model. We haven't been able to find a covariate that removes the bimodality, but note that R^\ddagger identifies the problem, the R^* do not.

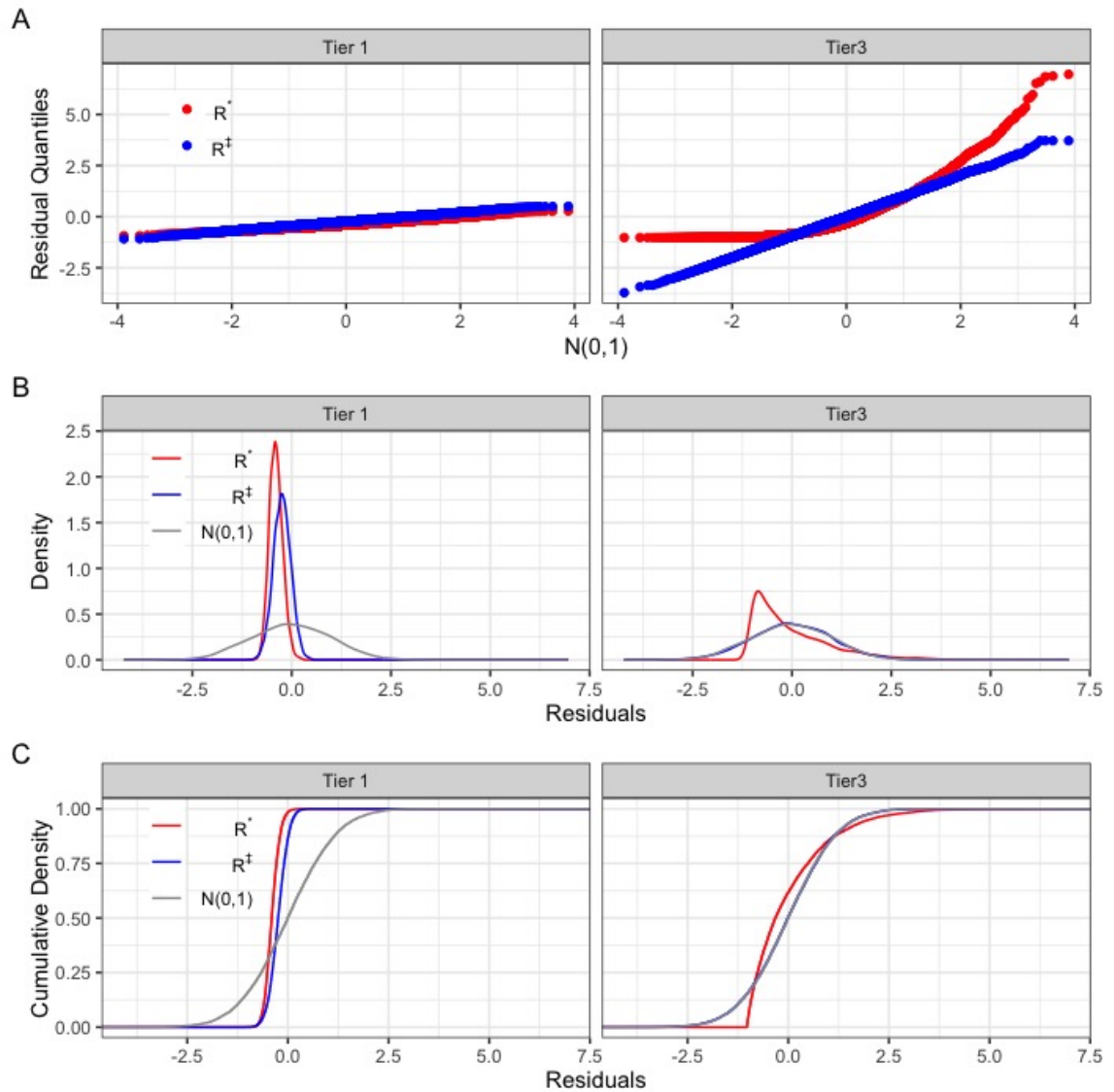


Figure 2: Distribution of the percentile location of Y_{fg} in its full posterior predictive distribution, Tier 1 (left column), Tier 3 (right column). Panel A, Q-Q plots; panel B, smoothed densities; Panel C, empirical CDFs. Panel A includes the reference $y = x$ line (black). Panels B and C include the reference $N(0,1)$ density and distribution.

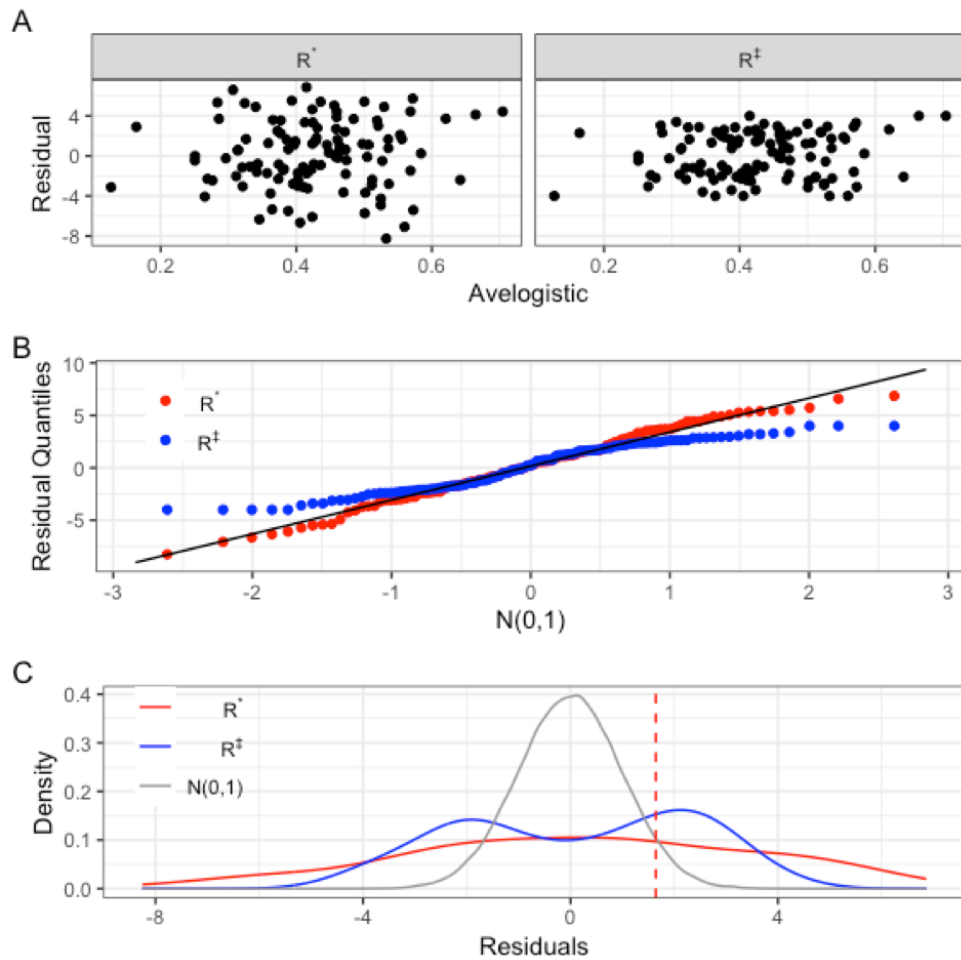


Figure 3: (A) R^* (left panel) and R^\dagger (right panel) vs avelogistic; (B) Q-Q Plots for R^\dagger and R^* residuals; (C) Histograms of R^\dagger and R^* residuals, along with the reference $N(0,1)$ density.

7 Discussion

Residuals are a mainstay for assessing model fit and detecting outliers. We define and evaluate a percentile-based approach that, by respecting all aspects of a predictive distribution, is a considerable improvement over use of the standard residuals. Improvements include properly calibrated Type I error when testing a working hypothesis, improved power, and more revealing diagnostic plots. While it is the case that the nominal α for testing can be adjusted to calibrate the standard residuals to have a desired Type I error, and with careful adjustments can improve residual plots and other model diagnostics, the percentile-approach automatically takes care of these issues. The percentile-based approach has the added benefit of encouraging development of a full predictive distribution that incorporates sampling, measurement, and modeling-induced uncertainties. Consequently, we encourage its use.

Funding

The authors gratefully acknowledge partial support from the following sources: SB, NIH-NIAID, U19-AI089680; QL, Performance Monitoring and Evaluation 2020 project from the Bill & Melinda Gates Foundation; CW, NCI P30CA006973, NCI 1 P50 CA098252; TAL, NIH-NIAID, U19-AI089680

Acknowledgments

The authors are grateful to the Southern and Central Africa International Centers for Excellence in Malaria Research for useful discussions particularly in relation to the section on applications to protein microarrays.

Bibliography

Cook, S. R., Gelman, A., and Rubin, D. B. “Validation of software for Bayesian models using posterior quantiles.” *J. Comput. Graph. Statist.*, 15:675–692 (2006).

- Dunn, P. K. and Smyth, G. K. “Randomized Quantile Residuals.” *Journal of Computational and Graphical Statistics*, 5(3):236–244 (1996).
- Efron, B. “Better Bootstrap Confidence Intervals.” *Journal of the American Statistical Association*, 82:171–185 (1987).
- . “Microarrays, Empirical Bayes and the Two-Group Model.” *Statistical Science*, 23:1–22 (2008).
- Gelman, A., Rubin, D. B., et al. “Inference from iterative simulation using multiple sequences.” *Statistical science*, 7(4):457–472 (1992).
- Li, Q., Louis, T. A., Liu, L., Wang, C., and Tsui, A. “Subnational estimation of modern contraceptive prevalence in five sub-Saharan African countries: a Bayesian hierarchical approach.” *BMC Public Health*, 19(1):216 (2019).
- Zimmerman, L., Olson, H., Tsui, A., and Radloff, S. “PMA2020: Rapid Turn-Around Survey Data to Monitor Family Planning Service and Practice in Ten Countries.” *Studies in Family Planning*, 48(3):293–303 (2017).